sensors

MDPI

Article

A Sensitive Pyrimethanil Sensor Based on Electrospun TiC/C Film

Ling Sui, Tingting Wu, Lijuan Liu, Honghong Wang, Qingqing Wang, Haoqing Hou and Qiaohui Guo *

Department of Chemistry and Chemical Engineering, Jiangxi Normal University, Nanchang 330022, China; 15079058173@163.com (L.S.); wtt1874983756@163.com (T.W.); 15979385750@163.com (L.L.); WHHong816@163.com (H.W.); Wyuan0816@yeah.net (Q.W.); zxp1014@126.com (H.H.)

* Correspondence: guoqiaohui@jxnu.edu.cn; Tel.: +86-791-8812-0389; Fax: +86-791-8812-0536

Received: 24 February 2019; Accepted: 26 March 2019; Published: 29 March 2019

Abstract: Titanium carbide (TiC) is a very significant transition metal carbide that displays excellent stability and electrical conductivity. The electrocatalytic activity of TiC is similar to noble metals but is much less expensive. Herein, carbon nanofibers (CNFs)-supported TiC nanoparticles (NPs) film (TiC/C) is prepared by electrospinning and carbothermal processes. Well-dispersed TiC NPs are embedded tightly into the CNFs frameworks. The electrochemical oxidation of pyrimethanil (PMT) at the TiC/C-modified electrode displays enhanced redox properties, and the electrode surface is controlled simultaneously both by diffusion and adsorption processes. When TiC/C is applied for PMT determination, the as-fabricated sensor shows good sensing performance, displaying a wide linear range (0.1–600 μM, R^2 = 0.998), low detection limit (33 nM, S/N = 3), and good reproducibility with satisfied anti-interference ability. In addition, TiC/C shows long-term stability and good application in natural samples. The facile synthetic method with good sensing performance makes TiC/C promising as novel electrode materials to fabricate efficient sensors.

Keywords: electrospinning; TiC; pyrimethanil; electrochemical sensor

1. Introduction

To control plant pests and other diseases, the usage of pesticides is widely relied upon [1]. Some of these pesticides are used for protecting food crops during cultivation and post-harvest storage. However, most of these chemicals may exist in the environment after their usage [2]. Therefore, residues of these pesticides would be discovered in fruits, vegetables, or water, which threaten human health. As one kind of aniline–epyrimidine fungicides, pyrimethanil (PMT, chemical structure shown in Scheme 1) plays a crucial role in agriculture, as it is applied to control leaf scab and some post-harvest diseases [3]. However, the wide usage of PMT would produce residues that may become a possible threat for health and environment. Due to the toxicity of PMT, the European Union Directive on drinking water quality established a maximum allowed concentration (0.1 μg/L) for PMT [4]. Therefore, developing a sensitive method to determine PMT is very important. Recently, PMT residues are monitored commonly by gas chromatography or high-performance liquid chromatography (HPLC) coupled with selective detectors [5–8]. These technologies display satisfactory accuracy, high reproducibility and reliability, but they are also subject to some inevitable shortcomings, such as the need for trained personnel, expensive instruments, and complex extraction steps. On the other hand, electrochemical methods have attracted much attention for the quantitative analysis of pesticide residues due to their good stability, high sensitivity, and low cost [9–11].

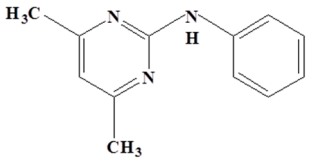

Scheme 1. The chemical structure of pyrimethanil (PMT).

Recently, transition metal carbides, such as TaC, TiC, and Mo_2C, have attracted growing attention due to their high catalytic activity. Additionally, the catalytic activity of these transition metal carbides is similar to that of noble metals, but they are less expensive. Particularly, as a vital transition metal carbide, TiC displays wide applications in supercapacitors [12], dye-sensitized solar cells [13], and lithium-ion batteries [14], owing to its good chemical and thermal stability, high catalytic activity, and low conductivity (6.8×10^{-5} Ω/cm). Recently, various TiC nanostructures, such as core–shell [12,15], nanowire [14], nanorod [16], and nanoparticle (NP) [17,18], have been widely exploited. Although TiC NPs can effectively improve its electrochemical activity, they tend to agglomerate, decreasing its specific surface area.

Herein, a hybrid of TiC NPs loaded carbon nanofibers (TiC/C) was synthesized via a simple electrospinning and carbothermal approach. Well-dispersed NPs were dispersed tightly on the skeleton of carbon nanofibers (CNFs). As expected, the TiC/C hybrid displayed superior sensing performance for PMT determination. In addition, TiC/C was also used for the detection of PMT in natural samples.

2. Experimental

2.1. Reagents

Titanium tetrachloride ($TiCl_4$), polyacrylonitrile (PAN), and polyvinylpyrrolidone (PVP, M_w = 1,500,000) were obtained from Sigma-Aldrich. PMT was purchased from Bepharm Co. Ltd. (Guangzhou, China). Phosphate buffer saline (PBS) was prepared by mixing 0.1 M NaH_2PO_4 and Na_2HPO_4. All of the solutions were dissolved with deionized water, obtained from a Milli-Q water purifying system (18 MΩ cm^{-1}). The water samples were obtained from a stream in Nanchang City (Jiangxi, China) and filtered with 0.50 μm nylon. Two kinds of food (apple and cucumber) were obtained from local supermarket. A part of apple and cucumber pericarp was cut up and added into beaker, and some ethanol was added to dissolve the pesticide residues. Assisting ultrasonic treatment was conducted for about 60 min, then the solution was filtrated for further experiments.

2.2. Apparatus

ATESCAN VEGA-3 scanning electron microscope (SEM) and a Tecnai G20 transmission electron microscope (TEM) were used to characterize the morphology of TiC/C. Raman spectroscopy (WITec-CRM200 Raman system with a laser wavelength of 532 nm) was used to characterize the microstructure of TiC/C. Thermogravimetric analysis (TGA) was performed on a SDT Q700 thermal analyzer (TA Instruments Co., Tokyo, Japan) under air atmosphere. Electrochemical experiments were tested on CHI 760 E electrochemical workstation (Shanghai, China). A three-electrode configuration was employed to performed electrochemical experiments, of which a platinum wire was used for auxiliary electrode. The reference electrode was Ag/AgCl (saturated KCl), and the bare glass carbon electrode (GC) was used as working electrode. Electrochemical impedance spectroscopy (EIS) was measured in 0.1 M KCl solution containing 5 mM $Fe(CN)_6^{3-/4-}$ (1:1). The frequency was 1.0×10^{-2} ~ 1.0×10^{5} Hz.

2.3. Preparation of TiC/C

TiC/C hybrid was synthesized by combination of electrospinning and carbothermal processes [19]. Briefly, $TiCl_4$ (12 wt% relative to $TiCl_4$) was dissolved in PVP ($TiCl_4$/PVP). PAN (18 wt% relative to PAN) was dissolved in DMAC (PAN/DMAC), then PAN/DMAC solution was mixed with $TiCl_4$/PVP

(1:1) solution with continuous string for 4 h at 60 °C. The electrospinning process was under a 30 kV voltage, and the nanofibers were collected onto a rotating drum. The as-electrospun nanofibers were oxidized at 230 °C (2 °C/min, 5 h, air atmosphere), and further thermal treatment at 1000 °C (10 °C/min, 1 h, vacuum). For a comparison, CNFs film (the electrospinning solution was PAN/DMAC without the addition of $TiCl_4$/PVP solution) was also prepared under the same condition.

2.4. Electrode Preparation

Glass carbon electrode (GC, θ = 3 mm) was polished carefully using Al_2O_3 powder. The electrode was rinsed and sonicated twice with distilled water and used for further experiments. An amount of 8 mg/mL of TiC/C was dispersed in a solvent mixture containing 25 µL of Nafion (5 wt%) and 250 µL of distilled water by sonication. Immediately after dispersion, 6 µL of TiC/C slurry was coated onto GC electrode surface (TiC/C/GC). The 0.1 M PBS solution was prepared by purging with high purity nitrogen (N_2) for 30 min and a N_2 blanket was maintained above the solution during measurement.

3. Results and Discussion

3.1. Characterization

TiC/C hybrid was synthesized from PAN/$TiCl_4$ nanofibers. During the carbothermal process, the nanofibers were carbonized into CNFs, and TiC NPs were formed in situ. Therefore, TiC/C hybrid was incorporated into one step. It can be seen from Figure 1A that TiC/C revealed 3D network structure, and TiC NPs were homogeneously dispersed on the surface of CNFs. The detailed morphology of TiC/C was further performed by TEM technique. The results showed that NPs were embedded into the CNF frameworks (Figure 1B).

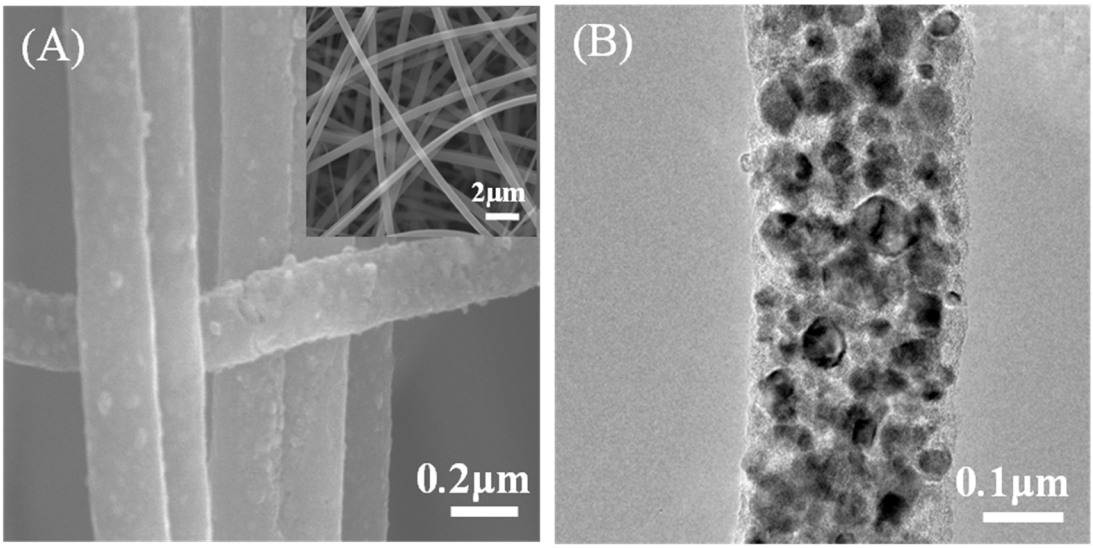

Figure 1. SEM (**A**) and TEM (**B**) images of TiC/C; Inset was the SEM image of CNFs.

The electrical conductivity of TiC/C film was evaluated via a four-point probe method using the following equation [19]:

$$\sigma = \frac{L}{RA} \quad (1)$$

where L is the distance between two electrode (cm), R is the resistance of TiC/C film (Ω), and A is the cross-sectional area of TiC/C film (cm^2). The electrical conductivity of CNFs was 0.50 $S{\cdot}cm^{-1}$. However, the electrical conductivity of TiC/C increased to 25.5 $S{\cdot}cm^{-1}$. The results revealed that TiC NPs embedded CNFs could enhance the percolation-type of conduction [20].

Raman spectroscopy is widely used to investigate the structure of molecule and crystal lattice. There were two strong peaks centered at 1338 and 1575 cm^{-1}, which were the graphite peaks of TiC/C, and other peaks at 264, 416, and 602 cm^{-1} corresponded to the TiC phase (JCPDS: 65–0242) (Figure 2A), confirming the formation of TiC nanocrystal. TGA analysis was used to measure the thermal stability of TiC/C. As shown in Figure 2B, a weight increase (250–550 °C) was obtained from TiC/C. The increase of weight was due to TiC oxidation into titanium dioxide (TiO_2) in air atmosphere ($TiC + 2O_2 \rightarrow TiO_2 + CO_2$) [19]. The amount of TiC was 40.3% in TiC/C, according to the change of weight [21]. Additionally, the temperature of 5% weight loss in TiC/C was 550 °C, which was higher than that of CNFs (390 °C), demonstrating that TiC/C owned much better thermal stability.

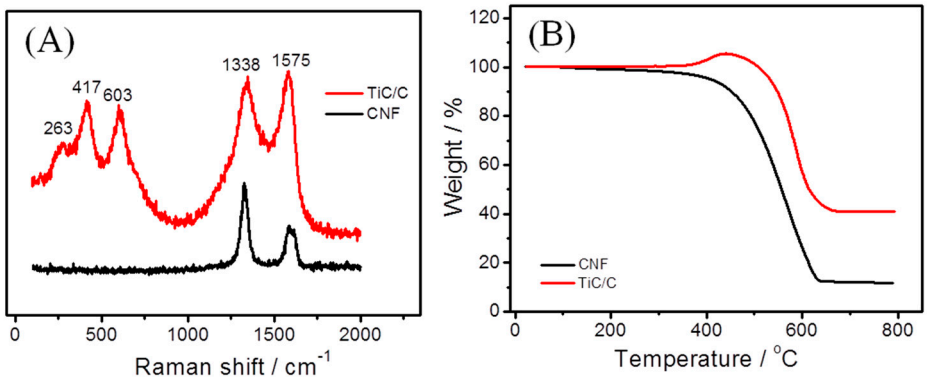

Figure 2. Raman spectra (**A**) and TGA curves (**B**) of TiC/C and CNF in air atmosphere.

3.2. Electrochemical Behavior

The electrochemical behaviors of PMT at TiC/C were systematically investigated. As shown in Figure 3A, there was a weak anodic peak centered at 1.13 V at bare GC. A strong anodic peak at 1.08 V could be seen at the CNFs-modified electrode. The peak current of CNFs increased compared with that of bare GC, attributing to the 3D network structure of CNFs, which increased the active area of the electrode. With regard to TiC/C, the anodic peak potential of PMT was observed at a lower potential (1.02 V), and the anodic peak current was almost twice compared to that of CNFs, suggesting that the electrocatalytic activity of TiC/C hybrid was improved with the introduction of TiC NPs. Meanwhile, no cathodic peak appeared in the reverse scan, indicating that the electrochemical process of PMT was irreversible. The results suggested that TiC/C might be employed as a PMT electrochemical probe with high catalytic activity.

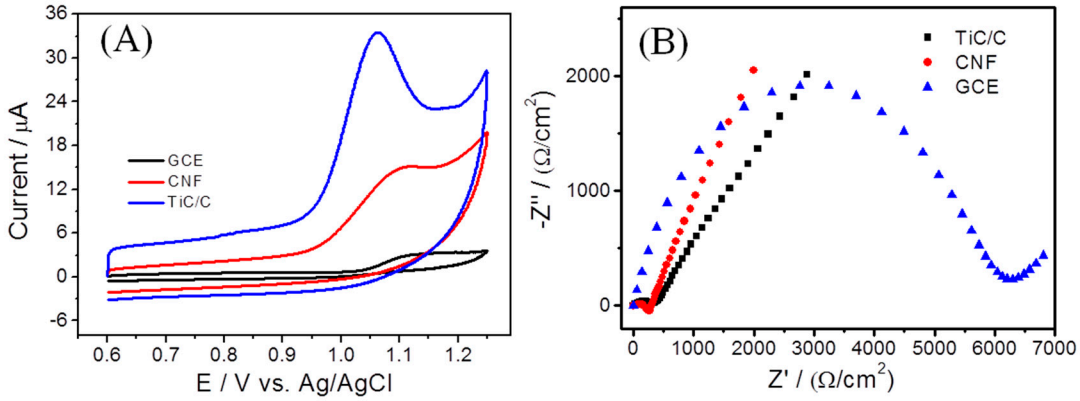

Figure 3. (**A**) CV curves of bare GC, CNFs, and TiC/C-modified electrodes in 0.1 M PBS (pH = 4.0) containing 50 μM PMT; (**B**) Nyquist plots of bare GC, CNFs, and TiC/C-modified electrodes.

The electrochemical impedance spectroscopy (EIS) was performed to analyze the surface properties of electrode. The electron transfer resistance (R_{ct}) values were 1.56×10^3, 1.23×10^3,

and 5.88 × 10^3 Ω/cm^2 for CNFs, TiC/C, and bare GC, respectively (Figure 3B). When CNFs was modified on the bare GC, the value of Rct decreased, indicating that CNFs formed a fast electron transfer pathway. In addition, the Rct of TiC/C was lower than that of the CNFs-modified electrode, indicating that TiC NPs could facilitate the electron transfer between TiC/C film and electrode surface.

3.3. Effect of pH

The effect of pH was investigated by CV. The peak current intensity increased from 2.0 to 4.0 and decreased when the pH value further increased (Figure 4A). Thus, pH 4.0 was selected as an optimal value. The plot of E_{pa} verus pH was linear, the regression equation was: E_{pa} (mV) = −56/Ph + 1.32 (R = 0.998) (Figure 4B). The obtained slope value (56 mV/pH) was close to the theory value (59 mV/pH), suggesting that identical numbers of protons and electrons participated in the reaction.

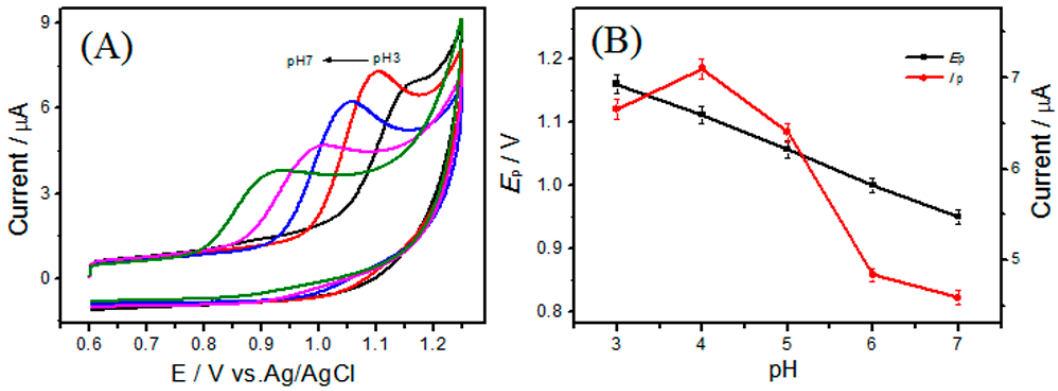

Figure 4. (**A**) CV curves of TiC/C-modified electrode in 0.1 M PBS in the present of 10 μM PMT with different pH values. (**B**) The effect of pH on the formal potential and anodic peak current.

3.4. Effect of Scan Rate

To assess the kinetic process, different scan rates for PMT oxidation were investigated. The peak potential shifted to positive when increased the scan rate (Figure 5A), suggesting that the electrochemical process was a kinetic limitation, and the current increased linearly with the square root of scan rate. The linear regression equation was: I_p (μA) = 5 + 115.6 $\nu^{1/2}$ (V/s, R = 0.999) (Figure 5B), suggesting that a diffusion-controlled process had taken place at TiC/C. Also, the plot of *log* I_p versus *log* ν was found to be linear (50–250 mV/s): *log* I_p = 1.42 + 0.62 *log* ν (R=0.993). The slope (0.62) was higher than the theoretical value (0.5), suggesting that this reaction was a diffusion-controlled process. However, the value was less than the theoretical value of 1.0 (adsorption-controlled process), illustrating that the oxidation of PMT at TiC/C also was an adsorption-controlled process [22,23]. The above results suggested that the oxidation of PMT at TiC/C was dominated by diffusion process accompanied by adsorption process [24].

For an irreversible reaction, the peak potential (E_p) is described as follows [25]:

$$E_p = E^0 + \left(\frac{RT}{\alpha nF}\right)\ln\left(\frac{RTk^0}{\alpha nF}\right) + \frac{RT}{\alpha nF}\ln v \quad (2)$$

The plot of E_p versus *ln* ν was linear, and its equation was: E_p (V) = 1.18 + 0.06 *ln* ν (R = 0.992) (Figure 5C). The calculated value of αn was 0.97. The electron number could be obtained from the Tafel curve. As shown in Figure 5D, the E_p was proportional to *log* ν, and could be described by the following equation: E_p (V) = 1.18 + 0.056 *log* ν (R = 0.996). The Tafel slope of b was obtained from the following equation [26,27]:

$$E_p = \frac{b(log\ v)}{2} + C \quad (3)$$

where

$$\text{Slope} = \text{b} = \frac{2.303RT}{(1-\alpha)nF} \quad (4)$$

The Tafel slope of b was calculated as 0.103. Therefore, the calculated electron transfer number (n) was 0.97 (close to 1). Thus, it could be inferred that one proton and one electron took part in the electrochemical reaction.

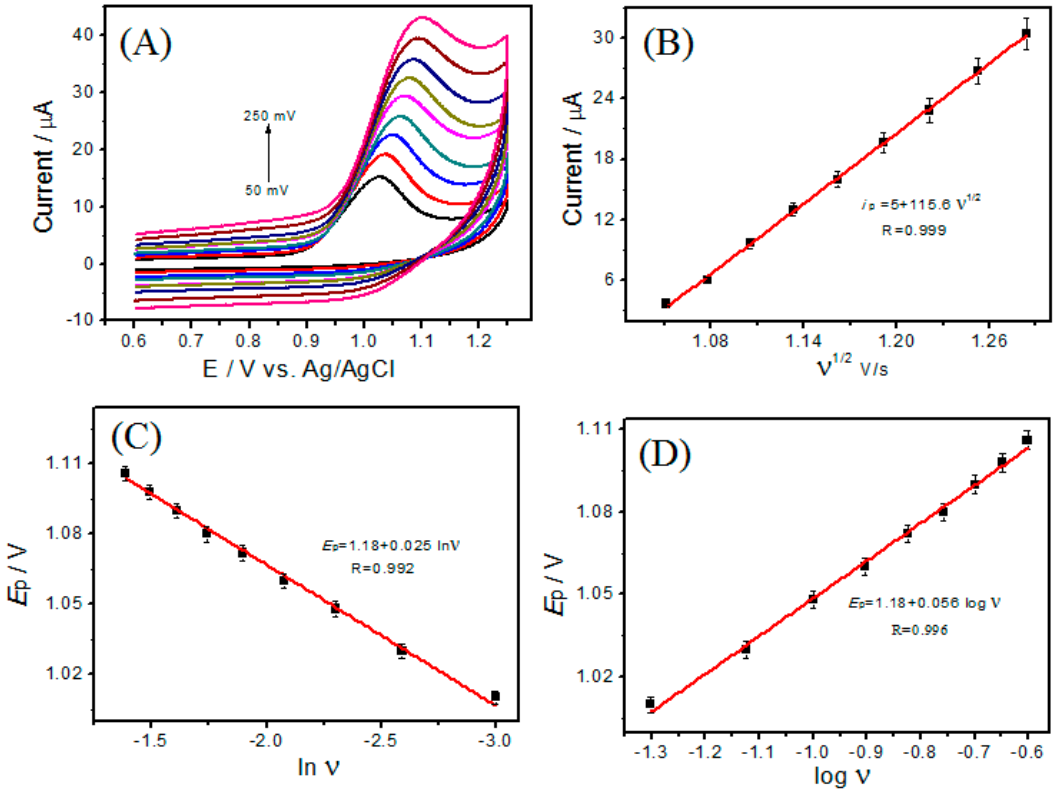

Figure 5. CVs of TiC/C with different scan rates, respectively (**A**); Dependence of peak current (I_p) versus $v^{1/2}$ (**B**); Dependence of E_p versus ln v (**C**); Dependence of E_p versus log v (D).

3.5. Determination of PMT by DPV

Figure 6A was the CVs of TiC/C with PMT ranging from 10 to 30 μM. The peak current increased when increasing PMT concentration. This result denoted that the effectively electrochemical sensing ability of TiC/C without fouling effect. As a sensitive electrochemical technique, DPV was selected for PMT determination. As expected, the peak current of PMT increased linearly with its concentration (Figure 6B). The linear range was 0.1–600 μM (R^2 = 0.998). The detection limit was 33 nM (S/N = 3). The linear equation was: I (μA) = 0.72 + 0.02 C_{PMT} (μM) (R^2 = 0.998) (Figure 6C). The sensing performances of PMT sensor were compared to other methods/materials (Table 1). The results displayed that the TiC/C exhibited a wider linear range or lower detection limit compared to the reported results [28–31], suggesting TiC/C was a promising material for PMT detection.

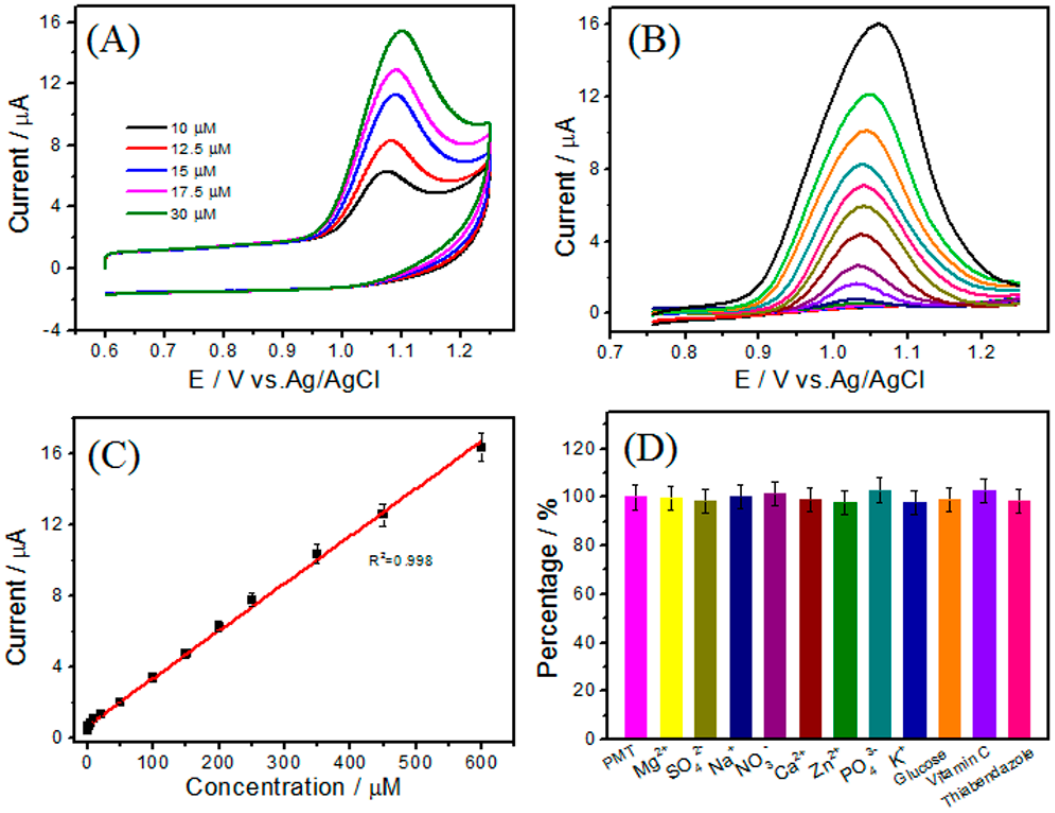

Figure 6. CVs (**A**) and DPVs (**B**) of TiC/C containing different concentrations of PMT; (**C**) is the calibration plot for PMT; (**D**) The percentage of interfering signals (NO_3^-, Mg^{2+}, SO_4^{2-}, Zn^{2+}, Ca^{2+}, Na^+, K^+, PO_4^{3-}, glucose, vitamin C, and thiabendazole) to PMT.

Table 1. Sensing performances of different methods/materials in the determination of PMT.

Methods	Linear Range (μM)	LOD (nM)	Ref.
Liquid chromatography	0.025–25	9.0	[28]
MWCNTs-[BMIM][PF6]	0.1–100	16.0	[29]
PANI-β-CD/fMWCNT	10–80	1040	[30]
NiCo2O4/RGO/[OMIM]PF6	0.1–140	11.0	[31]
TiC/C	0.1–600	33.0	This work

3.6. Reproducibility, Stability, and Interference Study

The reproducibility of the as-fabricated sensor was also evaluated. The relative standard deviation (RSD) for six electrodes was 3.4%. The RSD of each electrode for six measurements was 2.35%. To assess the stability of TiC/C, a day-to-day stability was investigated. Satisfied stability was found, and the RSD was less than 4.7%, demonstrating that the sensor possessed good reproducibility and stability. The acceptable stability of TiC/C can be due to the embedded TiC NPs, which could prevent NPs detachment and agglomeration from TiC/C frameworks.

The anti-interference ability is an important parameter for PMT detection. Some common compounds, such as NO_3^-, Mg^{2+}, SO_4^{2-}, Zn^{2+}, Ca^{2+}, Na^+, K^+, PO_4^{3-}, glucose, vitamin C, and thiabendazole, may coexist with PMT in the natural samples. Under the optimized conditions, the oxidization peak current of 50 μM PMT was individually measured in the presence of different interferents and their influence on the analytical signal was investigated. The results indicated that 50-fold concentration of thiabendazole, 100-fold concentrations of glucose and vitamin C, and 500-fold concentrations of NO_3^-, Mg^{2+}, SO_4^{2-}, Zn^{2+}, Ca^{2+}, Na^+, K^+, and PO_4^{3-} showed negligible influence

on the PMT (current signal change < 5%) (Figure 6D), indicating a good anti-interference ability of TiC/C.

3.7. Natural Sample Analyses

To evaluate the applicability of TiC/C sensor, water, apple, and cucumber were selected for quantitative analysis. Satisfactory recoveries (96.50–101.07%) and low RSDs (2.5–3.8%) were found (Table 2), indicating the acceptable reliability and applicability of TiC/C in analytical applications.

Table 2. Detection PMT in natural samples using standard addition method.

Sample	Added (μM)	Found (μM)	Recovery (%)	RSD[a] (%)
Water	0	Nd [b]	–	–
	100.00	99.54	99.54	2.8
	200.00	202.15	101.07	2.5
Apple	0	Nd [b]	–	–
	50.00	48.25	96.50	3.2
	100.00	98.06	98.06	2.8
Cucumber	0	Nd [b]	–	–
	200.00	202.05	101.03	3.1
	300.00	301.21	100.40	3.8

[a] Relative standard deviation for n = 3; [b] Mean of not detect.

4. Conclusions

TiC/C hybrid was fabricated for the determination of PMT. Homogeneous TiC NPs embedded into the CNFs framework was observed, which integrated the large surface area and unique 3D-networked structure of CNF with the good electrocatalytic activity of TiC NPs. The TiC/C-modified electrode showed an enhanced electrochemical response for the oxidation of PMT. Wide linear range (0.1–600 μM, R^2 = 0.998) and low detection limit (33 nM, S/N = 3) were obtained. In addition, TiC/C also showed long-term sensing stability and reproducibility. The TiC/C showed potential applications in the fabrication of electrochemical sensors.

Author Contributions: Data curation, L.S.; Formal analysis, L.S., T.W. and L.L.; Investigation, L.S., T.W. and L.L.; Resources, H.W.; Writing—Original Draft Preparation, H.W. and Q.W.; Writing—review and editing, L.S.; and H.H.; Project Administration, Q.G.; Funding acquisition, Q.G.; All the authors discussed the results and commented on the manuscript.

Funding: This work was supported by the National Natural Science Foundation of China (21864014 and 21405065), the Natural Science Foundation of Jiangxi Province, China (20171BAB213015), the Science and Technology Project of Jiangxi Province, China (20161BCB24005), Project funded by China Postdoctoral Science Foundation (2017M611703), and foundation of Jiangxi Educational Committee (GJJ170169).

Conflicts of Interest: The authors declare that they have no conflict of interest.

References

1. Ma, J.; Wang, S.; Wang, P.; Ma, L.; Chen, X.; Xu, R. Toxicity assessment of 40 herbicides to the green alga Raphidocelis subcapitata. *Ecotoxicol. Environ. Saf.* **2006**, *64*, 456–462. [CrossRef] [PubMed]
2. Miquel, A.S.; Arben, M.; Salvador, A. Pesticide determination in tap water and juice samples using disposable amperometric biosensors made using thick film technology. *Anal. Chim. Acta* **2001**, *442*, 35–44.
3. Baggiani, C.; Baravalle, P.; Giraudi, G.; Tozzi, C. Molecularly imprinted solid-phase extraction method for the high-performance liquid chromatographic analysis of fungicide pyrimethanil in wine. *J. Chromatogr. A* **2007**, *1141*, 158–164. [CrossRef]
4. Cheng, J.; Xia, Y.T.; Zhou, Y.W.; Guo, F.; Chen, G. Application of an ultrasound-assisted surfactant-enhanced emulsification microextraction method for the analysis of diethofencarb and pyrimethanil fungicides in water and fruit juice samples. *Anal. Chim. Acta* **2011**, *701*, 86–91. [CrossRef] [PubMed]

5. Xia, Y.; Cheng, G.; Guo, F.; Wang, X.; Cheng, J. In-syringe demulsified dispersive liquid-liquid microextraction and high performance liquid chromatography-mass spectrometry for the determination of trace fungicides in environmental water samples. *Anal. Chim. Acta* **2012**, *724*, 47–53. [CrossRef] [PubMed]
6. Yu, X.; Pan, L.; Ying, G.; Kookana, R.S. Enhanced and irreversible sorption of pesticide pyrimethanil by soil amended with biochars. *J. Environ. Sci.* **2010**, *22*, 615–620. [CrossRef]
7. You, X.; Wang, S.; Liu, F.; Shi, K. Ultrasound-assisted surfactant-enhanced emulsification microextraction based on the solidification of a floating organic droplet used for the simultaneous determination of six fungicide residues in juices and red wine. *J. Chromatogr. A* **2013**, *1300*, 64–69. [CrossRef]
8. Zhou, Y.; Han, L.; Cheng, J.; Guo, F.; Zhi, X.; Hu, H.; Chen, G. Dispersive liquid-liquid microextraction based on the solidification of a floating organic droplet for simultaneous analysis of diethofencarb and pyrimethanil in apple pulp and peel. *Anal. Bioanal. Chem.* **2011**, *399*, 1901–1906. [CrossRef] [PubMed]
9. Li, L.B.; Liu, D.; Shi, A.P.; You, T.Y. Simultaneous stripping determination of cadmium and lead ions based on the N-doped carbon quantum dots-graphene oxide hybrid. *Sens. Actuators B Chem.* **2018**, *255*, 1762–1770. [CrossRef]
10. Li, L.B.; Liu, D.; Wang, K.; Mao, H.P.; You, T.Y. Quantitative detection of nitrite with N-doped graphene quantum dots decorated N-doped carbon nanofibers composite-based electrochemical sensor. *Sens. Actuators B Chem.* **2017**, *251*, 17–23. [CrossRef]
11. Li, L.B.; Yu, B.; You, T.Y. Nitrogen and sulfur co-doped carbon dots for highly selective and sensitive detection of Hg(II) ions. *Biosens. Bioelectron.* **2015**, *74*, 263–269. [CrossRef]
12. Zhou, G.Y.; Xiong, T.R.; He, S.J.; Li, Y.H.; Zhu, Y.M.; Hou, H.Q. Asymmetric supercapacitor based on flexible TiC/CNF felt supported interwoven nickel-cobalt binary hydroxide nanosheets. *J. Power Sources* **2016**, *317*, 57–64. [CrossRef]
13. Zhao, Y.; Thapa, A.; Feng, Q.; Xi, M.; Qiao, Q.; Fong, H. Electrospun TiC/C nano-felt surface-decorated with Pt nanoparticles as highly efficient and cost-effective counter electrode for dye-sensitized solar cells. *Nanoscale* **2013**, *5*, 11742–11747. [CrossRef]
14. Cheng, K.; Yang, F.; Ye, K.; Zhang, Y.; Jiang, X.; Yin, J.; Wang, G.; Cao, D. Highly porous Fe_3O_4–Fe nanowires grown on C/TiC nanofiber arrays as the high performance anode of lithium-ion batteries. *J. Power Sources* **2014**, *258*, 260–265. [CrossRef]
15. Yao, Y.; Huo, K.; Hu, L.; Liu, N.; Cha, J.J.; McDowell, M.T.; Chu, P.K.; Cui, Y. Highly conductive, mechanically robust, and electrochemically inactive TiC/C nanofiber scaffold for high-performance silicon anode batteries. *ACS Nano* **2011**, *5*, 8346–8351. [CrossRef] [PubMed]
16. Tao, X.; Du, J.; Yang, Y.; Li, Y.; Xia, Y.; Gan, Y.; Huang, H.; Zhang, W.; Li, X. TiC nanorods derived from cotton fibers: chloride-assisted VLS growth, structure, and mechanical properties. *Cryst. Growth Des.* **2011**, *11*, 4422–4426. [CrossRef]
17. Zhou, G.; Xiong, T.; Jiang, S.; Jian, S.; Zhou, Z.; Hou, H. Flexible titanium carbide–carbon nanofibers with high modulus and high conductivity by electrospinning. *Mater. Lett.* **2016**, *165*, 91–94. [CrossRef]
18. Guo, Q.H.; Liu, L.J.; Wu, T.T.; Wang, Q.Q.; Wang, H.H.; Liang, J.Y.; Chen, S.L. Flexible and conductive titanium carbide carbon nanofibers for high-performance glucose biosensing. *Electrochim. Acta* **2018**, *281*, 517–524. [CrossRef]
19. Jiang, S.H.; Uch, B.; Agarwal, S.; Greiner, A. Ultralight, thermally insulating, compressible polyimide fiber assembled sponges. *ACS Appl. Mat. Interfaces* **2017**, *9*, 32308–32315. [CrossRef] [PubMed]
20. Flaherty, D.W.; May, R.A.; Berglund, S.P. Low temperature synthesis and characterization of nanocrystalline titanium carbide with tunable porous architectures. *Chem. Mater.* **2010**, *22*, 319–329. [CrossRef]
21. Guo, Q.H.; Wu, T.T.; Liu, L.J.; Hou, H.Q.; Chen, S.L.; Wang, L. Flexible and conductive titanium carbide–carbon nanofibers for the simultaneous determination of ascorbic acid, dopamine and uric acid. *J. Mater. Chem. B* **2018**, *6*, 4610–4617. [CrossRef]
22. Agarwal, S.; Jiang, S.H.; Chen, Y.M. Progress in the field of water-and/or temperature-triggered polymer actuators. *Macromol. Mater. Eng.* **2019**, *304*, 1800548–1800566.
23. Esmaili, R.; Nematollahi, D. Kinetic study of the oxidation of 4-Morpholinoaniline and N,N-Dialkyl-p-phenylenediamines in the presence of barbituric acids derivatives by digital simulation of cyclic voltammograms. *J. Electrochem. Soc.* **2012**, *159*, 792–799. [CrossRef]

24. Mashhadizadeh, M.H.; Talemi, R.P. A new methodology for electrostatic immobilization of a non-labeled single strand DNA onto a self-assembled diazonium modified gold electrode and detection of its hybridization by differential pulse voltammetry. *Talanta* **2013**, *103*, 344–348. [CrossRef]
25. Laviron, E. General expression of the linear potential sweep voltammogram in the case of diffusionless electrochemical systems. *J. Electroanal. Chem.* **1979**, *101*, 19–28. [CrossRef]
26. Beitollahi, H.; Tajik, S.; Biparva, P. Electrochemical determination of sulfite and phenol using a carbon paste electrode modified with ionic liquids and graphene nanosheets: application to determination of sulfite and phenol in real samples. *Measurement* **2014**, *56*, 170–177. [CrossRef]
27. Zargar, B.; Parham, H.; Hatamie, A. Electrochemical investigation and stripping voltammetric determination of captopril at CuO nanoparticles/multi-wall carbon nanotube nanocomposite electrode in tablet and urine samples. *Anal. Methods* **2015**, *7*, 1026–1035. [CrossRef]
28. Liang, P.; Wang, F.; Wan, Q. Ionic liquid-based ultrasound-assisted emulsification microextraction coupled with high performance liquid chromatography for the determination of four fungicides in environmental water samples. *Talanta* **2013**, *105*, 57–62. [CrossRef] [PubMed]
29. Yang, Y.; Wang, Q.; Zhang, M.; Zhang, S.; Zhang, L. An electrochemical fungicide pyrimethanil sensor based on carbon nanotubes/ionic-liquid construction modified electrode. *Food Chem.* **2015**, *187*, 1–6. [CrossRef] [PubMed]
30. Garrido, J.M.P.J.; Rahemi, V.; Borges, F.; Brett, C.M.A.; Garrido, E.M.P.G. Carbon nanotube b-cyclodextrin modified electrode as enhanced sensing platform for the determination of fungicide pyrimethanil. *Food Control* **2016**, *60*, 7–11. [CrossRef]
31. Yang, L.J.; Hu, Y.D.; Wang, Q.; Dong, Y.Y.; Zhang, L. Ionic liquid-assisted electrochemical determination of pyrimethanil using reduced graphene oxide conjugated to flower-like $NiCo_2O_4$. *Anal. Chim. Acta* **2016**, *935*, 104–112. [CrossRef] [PubMed]